



Numerical modeling of clog fragmentation during SEN clogging in steel continuous casting

H. Barati^{a,b,*}, M. Wu^{b,*}, S. Ilie^c, A. Kharicha^{b,d}, A. Ludwig^b

^a K1-MET, Franz-Josef Street 18, 8700 Leoben, Austria

^b Chair for Modeling and Simulation of Metallurgical Processes, Department of Metallurgy, Montanuniversitaet Leoben, Franz-Josef Street 18, 8700 Leoben, Austria

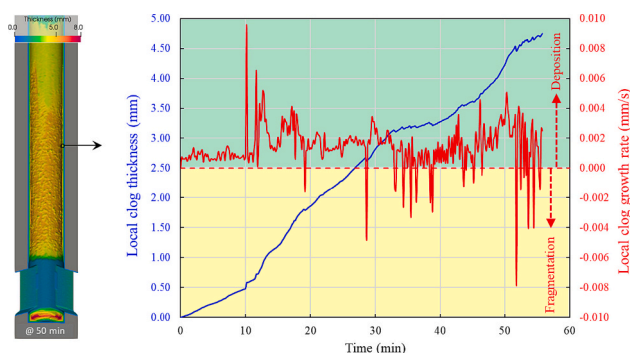
^c voestalpine Stahl GmbH, voestalpine-Straße 3, 4020 Linz, Austria

^d Christian-Doppler Laboratory for Metallurgical Applications of Magnetohydrodynamics, Department of Metallurgy, Montanuniversitaet Leoben, Franz-Josef Street 18, 8700 Leoben, Austria

HIGHLIGHTS

- A sub-model for the clog fragmentation was introduced and integrated into a comprehensive clogging model.
- Simulation of clogging/fragmentation in a real-scale SEN was conducted using the integrated clogging model.
- The simulation results were compared with the as-clogged SEN observed in steel plants.
- The importance of the fragmentation and necessity to have such a sub-model were affirmed.

GRAPHICAL ABSTRACT



ARTICLE INFO

Keywords:

Clogging
Continuous casting
Non-metallic inclusions
Fragmentation
Detachment

ABSTRACT

In the study of clogging during steel continuous casting, less attention was paid to the clog fragmentation, although it always accompanies the clogging process. This paper introduces a sub-model for the clog fragmentation integrated into a comprehensive transient clogging model. In this sub-model, the intricate network of the clog is simplified as a bunch of fictitious cylinders. Each cylinder, called 'clog finger', contains a column of spherical non-metallic inclusions (NMIs), which are mechanically bound by sintering at contact points. The mechanical stress acting at the sintering neck between NMIs due to hydraulic forces of the melt flow is evaluated. Simulation of clogging/fragmentation in a real-scale SEN was conducted using the integrated clogging model. Comparing the simulation results with the as-clogged SEN observed in steel plants revealed a qualitative agreement. The effects of different parameters were discussed. The importance of the fragmentation and necessity to have such a sub-model were affirmed.

* Corresponding author at: K1-MET, Franz-Josef Street 18, 8700 Leoben, Austria.

E-mail addresses: hadi.barati@k1-met.com (H. Barati), menghuai.wu@unileoben.ac.at (M. Wu).

<https://doi.org/10.1016/j.powtec.2023.119307>

Received 5 September 2023; Received in revised form 11 December 2023; Accepted 18 December 2023

Available online 19 December 2023

0032-5910/© 2023 Elsevier B.V. All rights reserved.

1. Introduction

As shown in Fig. 1(a), in continuous casting (CC) of steel, submerged entry nozzle (SEN) conveys the melt from the tundish to the mold, protects the melt from oxidation and stabilizes the CC process. However, a problem of clogging, i.e. build-up of solid materials on the inner wall of the SEN, could destabilize the process, hence deteriorate the casting quality. Another commonly accompanying issue in the clogging process is the fragmentation, i.e. detachment of fragments from the clog. From the online-monitored CC parameters, Fig. 1(b), it is found that the stopper position must be consistently adjusted to maintain the constant casting speed. When the flow passage inside the SEN is narrowed due to clogging, the stopper position is raised. In opposite, the lower-down of the stopper position indicates the occurrence of clog fragmentation. The detached clog fragments can act as new inclusions, being brought back into the steel melt. A positive consequence is that those fragments have relatively large size, are easier to float up and finally captured by the mold slag at the meniscus. A worse case could also occur, as shown in Fig. 1(c), that some fragments may go down with the melt flow and be captured by solidifying shell, leading to serious casting defects [1]. Numerous studies were done for the clogging in different fields of research [2–5], but in steel continuous casting less attention was paid to the clog fragmentation during the process.

Previous researches have proposed possible clogging mechanisms: deposition of non-metallic inclusions (NMIs) [7–9], reaction at the SEN wall [10–12], and temperature drop of the SEN leading to solidification of steel or precipitation of alumina [13–15]. Among them, the NMI deposition on the SEN wall is still considered as the primary cause for the clogging [16]. Based on previous knowledge, the clogging event can be divided into the following 6 steps: (a) formation of the first oxide layer by chemical reactions in the SEN refractory and at the steel-refractory interface; (b) transport of NMIs by turbulent melt flow; (c) interactions between the flow and the SEN wall, and adhesion of the NMIs on the SEN wall or on the clog front; (d) clog growth by the NMI deposition on the clog front and the flow-clog interactions; (e) fragmentation/detachment of the clog; (f) solidification of entrapped steel deep inside the clog.

Clogging has been studied by experiments and models. In experimental studies, characteristics of different material groups, like clog [10,17], non-metallic inclusions [2,18] and steel melt [19,20], were made and they were correlated to clogging phenomena.

Various numerical models have been developed by considering one or more main steps of clogging: Single-phase-based Eulerian approach [16,21,22], Eulerian-Lagrangian approach [23–26], and Eulerian-Eulerian two-phase approach [27,28]. These CFD models used the already adapted SEN geometry to study clog effects on flow, i.e. a part of step (d), or to study the transport of NMIs by turbulent melt flow, i.e. step (b). Computational thermodynamics has also been adopted to investigate reactions and inclusion formation [7,29–31]. Physical models using water as analog for steel have also been conducted to study the effects of as-clog SEN on the mold flow [32,33]. The current authors have developed a transient model for SEN clogging in steel CC that covers most critical clogging steps: chemical reactions on the SEN refractory called ‘early-stage’ of clogging [34], i.e. step (a), the clog growth due to NMI deposition called ‘late-stage’ of clogging [35–37], i.e. steps (b)–(d), and the possible solidification of entrapped steel, i.e. step (f). The model was validated with laboratory experiments [35] and its accuracy and efficiency were verified for industry SENs [37]. Unfortunately, no numerical model for the step (e) fragmentation is available. Only very few theoretical and experimental analyses about the fragmentation were reported [14,38].

In another research discipline, models for the detachment of deposit (also called ‘re-entrainment’, ‘resuspension’, or ‘removal’) such as soil particles, dust, and aerosolized drug particles were reported [39]. Nevertheless, there are two main difficulties in the modeling of multi-layer resuspension: deposit morphology and rupture mechanisms associated with the resuspension of large aggregates. There are several approaches to handle multilayer resuspension, like empirical formulas [40], force-balance [41], probability density function (PDF) [42,43], and fully Lagrangian [44]. However, they are not suitable for the application of real scale clogging in steel continuous casting due to following reasons: time-dependent sintering bonding between NMIs, unfeasible tracking of individual NMIs in clog, large size of CFD domain, and huge number of NMIs in the domain, etc.

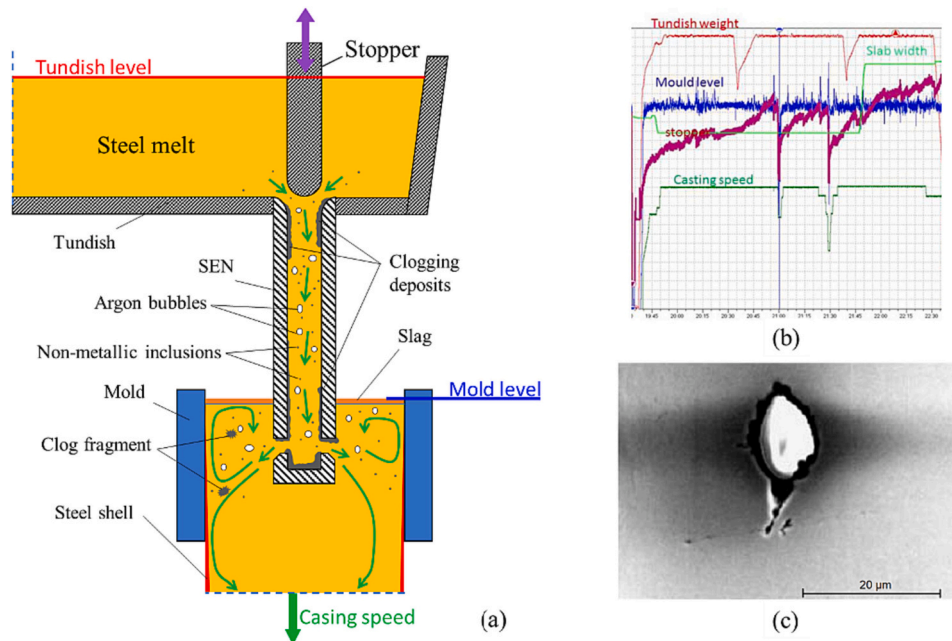


Fig. 1. Illustration of the clogging and fragmentation phenomena in SEN during CC. (a) Schematic of the multiphase flow, transport of non-metallic inclusions and clog fragments (b) Online monitoring of CC parameters (tundish weight, mold meniscus level, stopper rod position, casting speed) indicates the occurrence of clogging/fragmentation events [6], Copyright 2020, European Union; (c) Evidence about the possible entrapment of clog fragments in the solidified steel [1], Copyright 2008, EDP Sciences.

In this work a sub-model for the fragmentation during SEN clogging is proposed, i.e. step (e), and integrated in the comprehensive clogging model, targeting the engineering process of CC of large domain.

2. Modeling

2.1. Framework of the transient clogging model

SEN clogging usually occurs in two stages: in the ‘early-stage,’ the initial solid layer is built due to chemical reactions and it covers the refractory surface, and in the ‘late-stage’ the porous medium of clog grows by the continuous NMI deposition.

A 1D mathematical sub-model is used to calculate the thickness of the first oxide layer during the early-stage of clogging [34]. In this sub-model, the melt pressure and composition of the SEN refractory are considered for calculating the growth rate of the oxide layer in continuous casting of Ti-stabilized ultra-low-carbon (Ti-ULC) steel. The early-stage of clogging, controlled by melt–refractory reactions, prepares the surface, for the further deposition of suspended NMIs during the late stage of clogging, as shown in Fig. 2. Details of this mathematical formulation and its combination with late stage clogging model were explained previously [34].

To model the late stage of clogging an Eulerian approach was employed to calculate the turbulent melt flow in the SEN and a Lagrangian approach was used to track the motion of the NMIs. In addition, a volume-average scheme was used to define the clog as a porous medium and track the growth of the clog. In this finite volume model, computational cell can be ‘fully-clogged,’ ‘partially-clogged,’ or ‘free-of-clog’. In free-of-clog cells, NMIs are transferred in melt flow; drag, lift, virtual mass, and pressure gradient forces are considered; random-walk model is used to take turbulence effects into account. In fully-clogged cells, the flow and turbulence are damped using a Darcy source term for porous medium. In partially-clogged cells, a uniform layer of clog is assumed to cover the mutual cell faces with neighboring fully-clogged cells or wall. When an NMI enters a partially-clogged cell, it can attach to the clog, if its distance to the front of the clog layer is smaller than its radius. By the attachment, the NMI is removed from the

partially-clogged cell and its volume is added to the particle volume fraction of the cell, as shown in Fig. 2. Details of this model can be found in [35].

2.2. Sub-model for clog fragmentation

The concept of the sub-model for clog fragmentation is schematically described in Fig. 3. Following the metallographic analysis of as-clogged SEN [22,45], the clog structure is treated as a porous medium formed by random deposition of NMI particles, Fig. 3(a). The particles are bound together by high temperature sintering. When flow passes through the porous medium, hydraulic (drag) forces acting on the particle network would lead to a mechanical fracture at the weakest point of the sintering bound, i.e. fragmentation occurs. In the current clogging model, it is not feasible to calculate hydraulic forces on such a complex network, and it is also difficult to find the weakest point of the sintering bound. The following assumptions and modeling steps are made.

- 1) The intricate network of the clog is simplified as a bunch of fictitious cylinders, Fig. 3(b)-(c). Each cylinder, also called ‘clog finger’, contains a cluster of spherical NMI particles of equal diameter ($d_p = 2r_p$). Here the NMI is assumed as Al_2O_3 .
- 2) The length of the clog finger (L_c) increases with the continuous NMI deposition.
- 3) In each clog finger, NMI particles are mechanically bound by sintering at their contact points. The radius of the bound neck between NMI particles (r_n) increases with time due to the sintering, Fig. 3(c). Therefore, the neck radius along the clog finger is different between different spheres due to the different deposition time.
- 4) The flow is assumed perpendicular to the clog finger. The stress due to the hydraulic (drag) force of the melt flow at different points of each ‘clog finger’ can be derived. Weakest points of a ‘clog finger’ are at the sintering necks. Hence, the stress at each sintering bound neck (σ_n) is calculated.
- 5) Fragmentation of the clog finger occurs at the weakest point, when its stress exceeds the mechanical strength of alumina. The mass of the clog finger fragment is removed from the clog and the particle

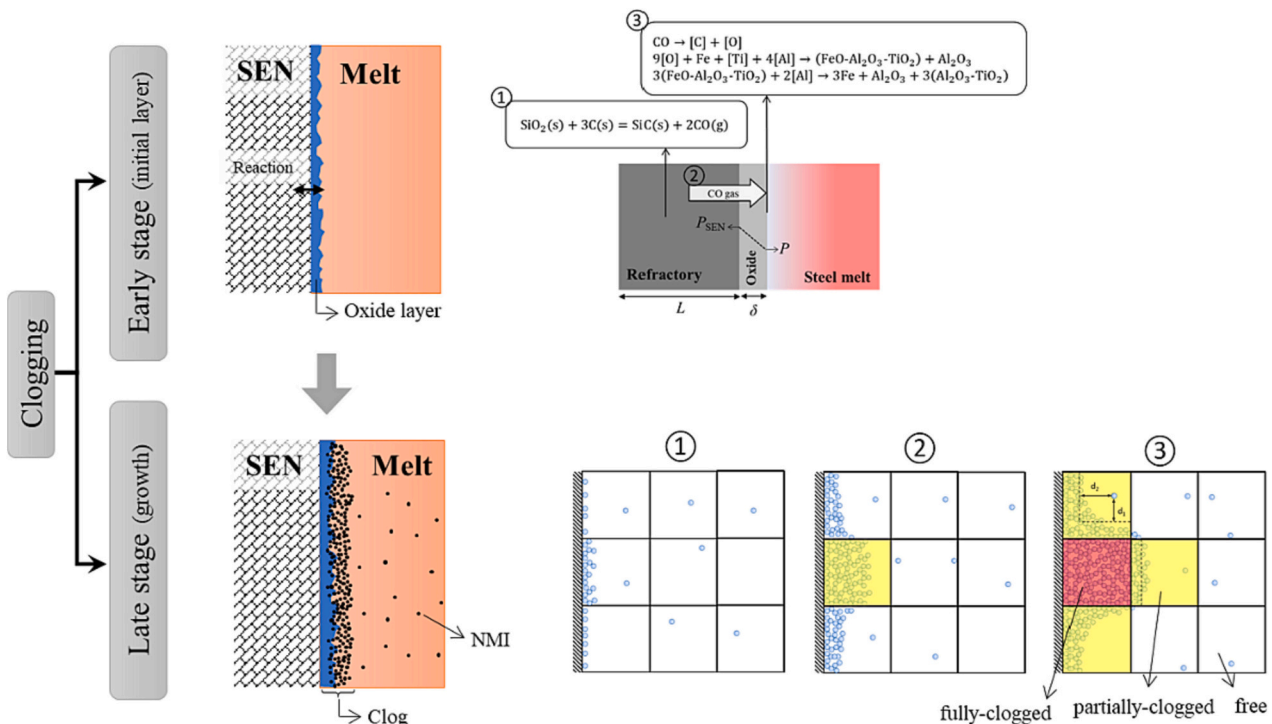


Fig. 2. Concept of the two-stage clogging.

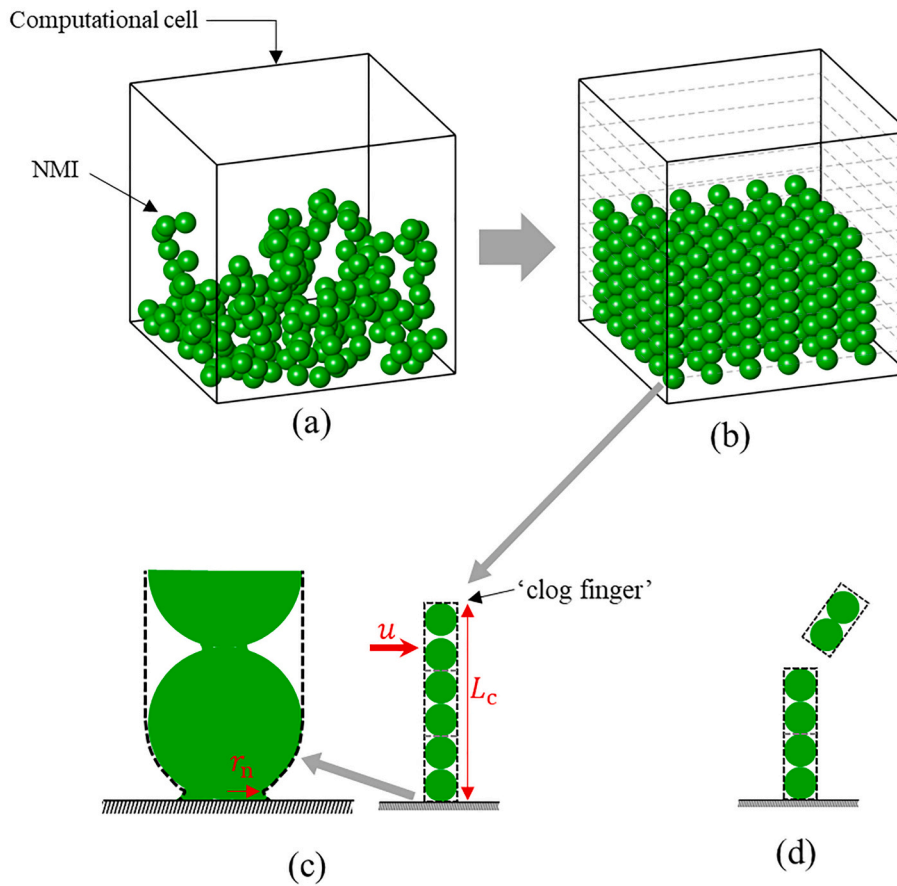


Fig. 3. Modeling concept for the clog fragmentation. (a) Clog network constructed by random deposition of NMIs, (b) simplification of the clog network as a bunch of uniformly distributed clog fingers, (c) graphical description of the clog finger as fictitious cylinder, (d) breaking of part of the clog finger.

fraction in the computational cell is updated. The remaining part of the clog finger can continue to grow with the NMI deposition.

6) Ideally, the stress should be calculated at each sintering point. However, it is not computationally feasible, because size of NMI is much smaller than the computational cell size. Here, each computational cell is virtually divided into M sections, illustrated by gray dashed lines in Fig. 3(b), and stress is only calculated at the base of each section.

The maximum stress on the base of each section of a clog finger (σ_n) is calculated according to Pilling and Hellowell [46], who have used the similar idea to calculate the stress at the base of a dendritic arm during alloy solidification. They considered the dendrite as a cylinder with different radii between the root and main section.

$$\sigma_n = \frac{2FL_c^2}{\pi r_n^3} \quad (1)$$

where $F = 3\pi\mu u_{\text{por}}$ is the total force acting on the clog finger by the melt flow. u_{por} is the velocity inside the pores of the clog network which is calculated based on total velocity magnitude in the computational cell (u) and clog fraction (f_{clog}) using an empirical formulation, $u_{\text{por}} = u f_{\text{clog}}^2$. μ is viscosity of the melt. Neck radius can be calculated by the theory of the kinetic growth of sintering neck of spheres,

$$\frac{r_n^m}{r_p^n} = A_{(T)} t \quad (2)$$

where $A_{(T)}$ is a temperature-dependent coefficient,

$$A_{(T)} = \frac{K_1 \gamma V_0 D}{RT} \quad (3)$$

In this equation, K_1 is a constant; γ is the interfacial tension; V_0 is the molar volume; D is the self-diffusion coefficient of the material; R is the gas constant; and T is the temperature. The exponents m and n in Eq. (2) define the sintering mechanism. Here, $m = 5$ and $n = 2$ according to the experimental observation of sintering alumina spheres in steel melt [47] showing that volume diffusion is the major mechanism of sintering. The self-diffusion coefficient of alumina (D) is a function of temperature that can be obtained by an Arrhenius equation, $D = D_0 \exp(-Q/RT)$. D_0 is a pre-exponential factor and Q is the activation energy.

In the current fragmentation sub-model, the diameter of the clog finger is much smaller than typical computational cell size. Hence, there is a forest of clog fingers with the same distance from each other. Tracking real number of NMIs is computationally infeasible; therefore, a statistical weight, called also N-factor, must be introduced to reduce the calculation cost. In fact, statistical weight refers to the number of representative particles. Considering simulation settings in this work, statistical weight was set to 8750. For average size of a cell, 0.70 mm, with deposition of one numerical particle, around two layers of real particles were added to the clog finger forest. Fracture of a clog finger occurs at the sintering joints between particles, where the stress exceeds its mechanical strength. Considering all joints in the calculation requires is also computationally costly, and it would need too much memory to store the time for each sintering join. The stress on each join depends on the neck radius, which is in turn the function of the time, as expressed in Eq. (1)–(2). Therefore, each cell was virtually divided to $M = 10$ sections in the clog growth direction. In other words, stresses were calculated at maximum 10 points of a clog finger. In a cell with average size of 0.70

mm, maximum 70 particles with 0.010 mm diameter can be filled in a clog finger. That is 7 particles in each section. This sectioning approach makes the computation feasible.

2.3. Simulation settings

A comprehensive model including both early and late stages of clogging as well as fragmentation was considered to simulate the clogging in a real scale SEN. Dimensions of the computational domain with boundary conditions are shown in Fig. 4. To have a more physical flow pattern at SEN ports, a part of mold was also included in the domain. It should be mentioned that in this paper flow in the mold region is not of main interest; therefore, a short part of mold was considered for sake of calculation costs. At the inlet, the mass flow rate of steel melt was 53.82 kg/s. Spherical alumina particles were injected with zero velocity and a mass injection rate of 0.0034 kg/s, corresponding to an oxygen content of 30 ppm in the steel melt in the tundish before entering SEN. The particle size was 10 μm . Non-slip flow boundary conditions were considered for walls of SEN and CC mold and a shear-free wall was set for the free surface (mold meniscus). The pressure outlet was set at the outlet. A hexahedral mesh was created for whole domain with finer mesh inside the SEN. The minimum and maximum cell volume in the SEN was 3.53×10^{-10} and $5.04 \times 10^{-9} \text{m}^3$, respectively. The physical properties and other parameters used in the simulations are summarized in Table 1.

The melt flow was calculated by solving Navier-Stokes equations. Scale Adaptive Simulation (SAS) and shear-stress transport (SST) $k-\omega$ turbulence models were adopted. Lagrangian tracking of solid NMI particles was done based on the balance of various forces including Buoyancy, drag, lift, virtual mass and pressure gradient. Details of the equations can be found in the previous publications [34,35].

The commercial computational fluid dynamics (CFD) code ANSYS-FLUENT was used to solve equations with extended user-defined functions (UDF) for considering tracking, attachment, and detachment of solid particles as well as the growth of the clog. Computations are done on a high-performance computer cluster with 30–48 CPUs (2.6 GHz). A simulation of a one-hour period of the process took approximately 12 days.

3. Results

A short simulation of only 15 s of the process was done with a fresh SEN, i.e. ignoring chemical reaction at melt-refractory interface (early-stage clogging) and NMI deposition (late-stage clogging). The time-averaged flow pattern is depicted in left hand side of Fig. 5. There are

Table 1

Physical properties, process and numerical modeling parameters.

Property/Parameter	Unit	Value
General clogging model		
Density of steel melt	kg m^{-3}	7030
Viscosity of steel melt	Pa s	0.006
Density of alumina inclusions	kg m^{-3}	3700
Early-stage sub-model		
Operating temperature	K	1822
Permeability of initial oxide layer	m^{-2}	10^{-17}
CO production rate by the SEN refractory	kg/s m^{-3}	0.048
Refractory thickness of the SEN	m	0.02
Initial roughness of SEN wall	m	10^{-5}
Fragmentation sub-model		
Strength of alumina at operating temperature	MPa	100
Interfacial energy (alumina – steel melt)	N m^{-1}	1.0
Molecular volume of alumina	$\text{m}^3 \text{mol}^{-1}$	2.56×10^{-5}
Pre-exponential factor (D_0)	$\text{m}^2 \text{s}^{-1}$	4.6×10^{-2}
Diffusion activation energy of alumina (Q)	J mol^{-1}	464.0×10^3
Number of virtual sections in cell (M)		10
Constant K_1	–	80

two inclined rotating jets passing through the two ports. These two jets are almost symmetric, and they are divided into two halves ‘A’ and ‘B’. However, the instantaneous flow is very transient and the rotating vortices vary frequently, as shown in right hand side of Fig. 5.

In the early stage of clogging, the initial oxide layer forms because of reactions at the interface between the molten metal and the refractory material. Once the oxide layer reaches a critical thickness, here around 0.1 μm , it serves as a substrate for the deposition of NMIs. Afterwards, both the reaction and NMI deposition processes, corresponding to the early and late stages of clogging, respectively, occur simultaneously, contributing to the further development of the clog. The early-stage clogging, i.e. the chemical reaction, terminates due to the pressure increase on the SEN refractory with the clog growth. Faster deposition of NMIs results in sooner termination of the early-stage [34]. Fig. 6(a) displays the termination time of the early-stage clogging in the boundary cells. A gray color indicates that the early stage has not terminated yet. Fig. 6(b) illustrates the contribution of the early-stage to the total clog thickness, which is represented by the ratio (or thickness fraction) between the oxide layer thickness and the overall clog thickness. A faster deposition rate of NMIs in the port region leads to an earlier termination of the early-stage and, consequently, a reduced contribution of the early stage to the total clog thickness. In the tube part of the SEN, the random distribution of termination times reflects the stochastic nature of NMI deposition. While the process conditions in the early stage, like pressure, are almost identical for all cells at a certain height of the SEN, the

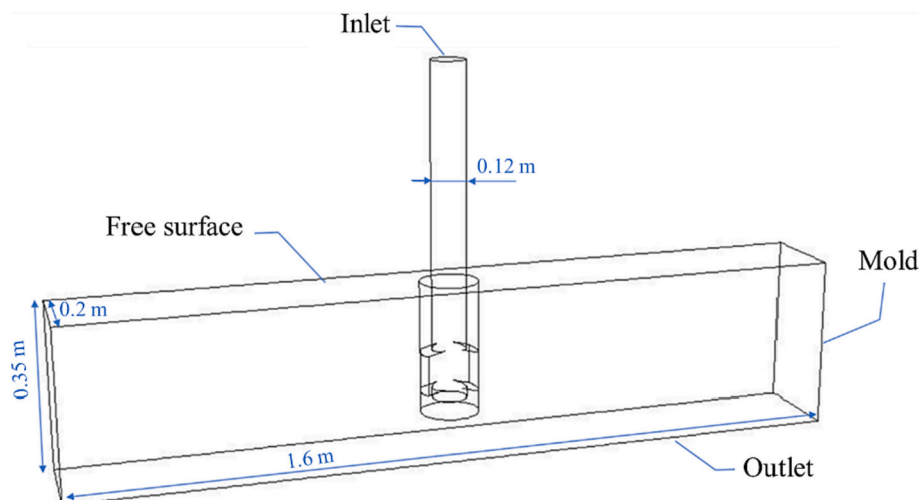


Fig. 4. Computational domain and notation of boundaries.

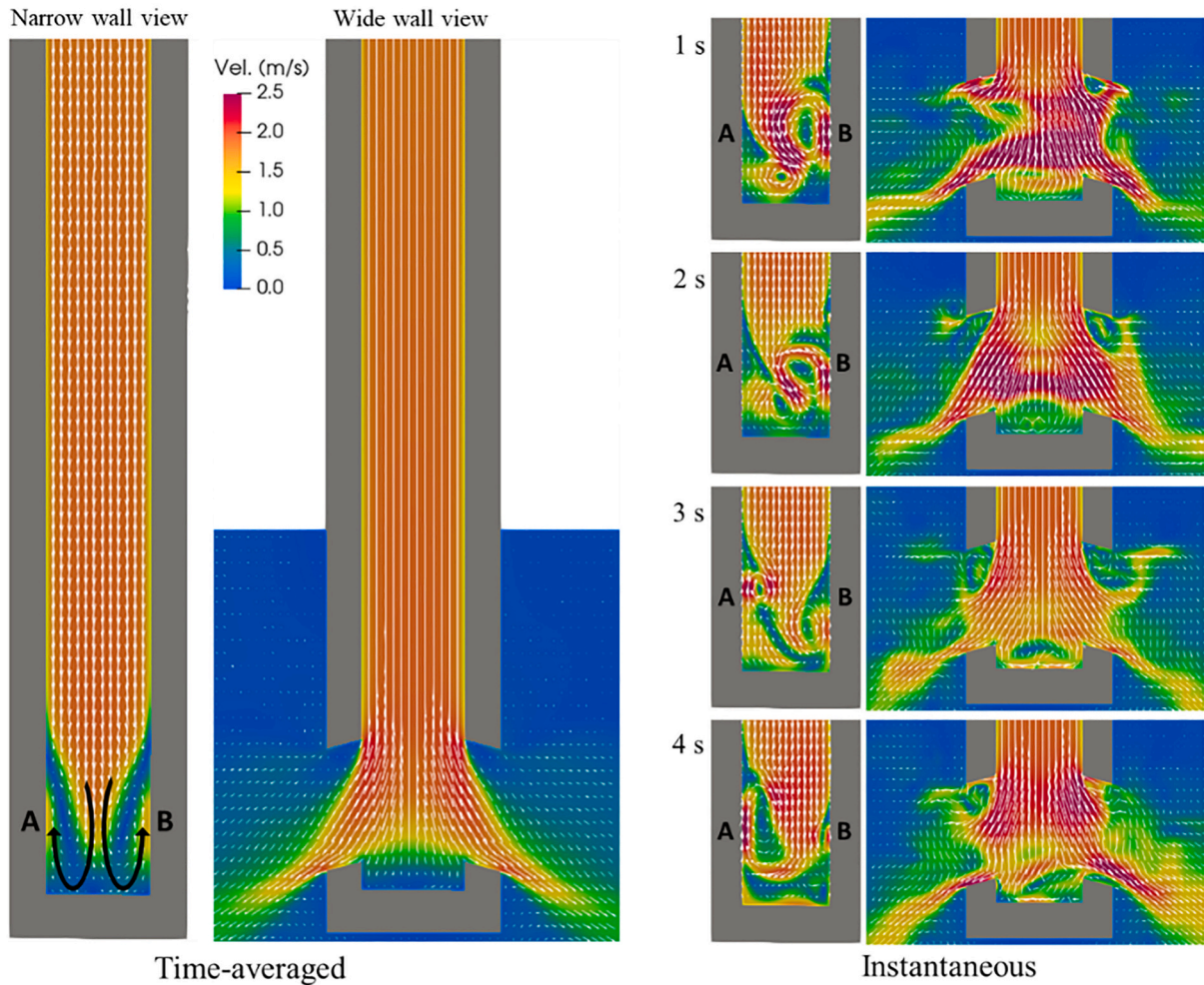


Fig. 5. Time-averaged flow pattern inside the fresh SEN over 15 s (left) and instantaneous flow sequences (right). The velocity magnitude is linearly scaled by vector length and color map.

random NMI deposition introduces erratic behavior in the early stage of clogging.

The further CC process with SEN clogging of around 1 h was simulated. Clogging evolution is depicted in Fig. 7. The SEN is cut through the wide symmetrical plane in two halves 'A' and 'B', and the clog thickness seems to distribute differently on the two halves. The clog thickness is defined by the distance between the SEN wall and the clog front. The turbulent flow resulted in formation of random bulges on the clog front. Investigation of clog sequences with smaller time intervals showed that bulges appear and disappear frequently due to the alternate deposition of NMIs and fragmentation of the clog. NMI deposition formed an almost thin layer of clog on the wall in the port region. At the bottom of SEN, clog grew faster at the corner. With the evolution of clogging, unsymmetrical growth of the clog became more visible. For example, at 50 min, the clog distribution is obviously different in two halves, especially in the upper tube part.

Less clogging on the top of the SEN tube is due to the inlet boundary conditions. At the inlet, particles were injected randomly in a circular area whose diameter is a little smaller than that of the SEN cross section. The random distribution of particles at the inlet was updated every time step. It took a while to transport particles from injection area to the SEN wall, i.e. it took some distance for particles to reach the wall on the top area of the SEN. To exclude effects of inlet boundary conditions on further analysis of clogging, the upper 40% of SEN was not considered in calculation of total deposition and fragmentation mass.

In Fig. 8, flow fields during the process are shown on two

symmetrical planes of the SEN. As the clogging velocity magnitude progresses, the velocity magnitude in the entire SEN increases. In this work, the inlet mass flow rate of the steel melt was kept constant to maintain a constant casting speed and a stable meniscus level. With the narrowing of the flow passage in the SEN, the velocity and consequently the turbulence enhanced. Similar to the fresh SEN case (Fig. 5), rotating vortices in the port region changed dynamically. Although the flow is very dynamic. This flow dynamics may be the cause leading to the unsymmetrical distribution of clog. However, the simulation results show that the response time of clog growth seems much slower than the flow dynamics.

The local fragmentation rate in the clog front cells at 50 min is illustrated in Fig. 9. Fragmentation rate is larger in the port region because of larger velocity of the melt flow in this region. Indeed, the melt flow washed most of the deposit from the SEN wall and only a thin layer remained there. Similar phenomenon was seen in the middle bottom of the SEN where the vertical stream hit the bottom of SEN. Hence, clogging proceeded from the corner and formed a bowl shape deposit. In the tube part of the SEN, the fragmentation rate in most of the clog front cells is very low. There are also scattered cells with larger fragmentation rate representing bulges.

The variation of the total masses of deposited and fragmented NMIs over time is shown in Fig. 10(a). The difference between the deposition and fragmentation masses defines the clogging mass. Although the curves in Fig. 10(a) look almost linear, their actual change rates vary dramatically, as shown in Fig. 10(b). In fact, the curves in Fig. 10(b) are

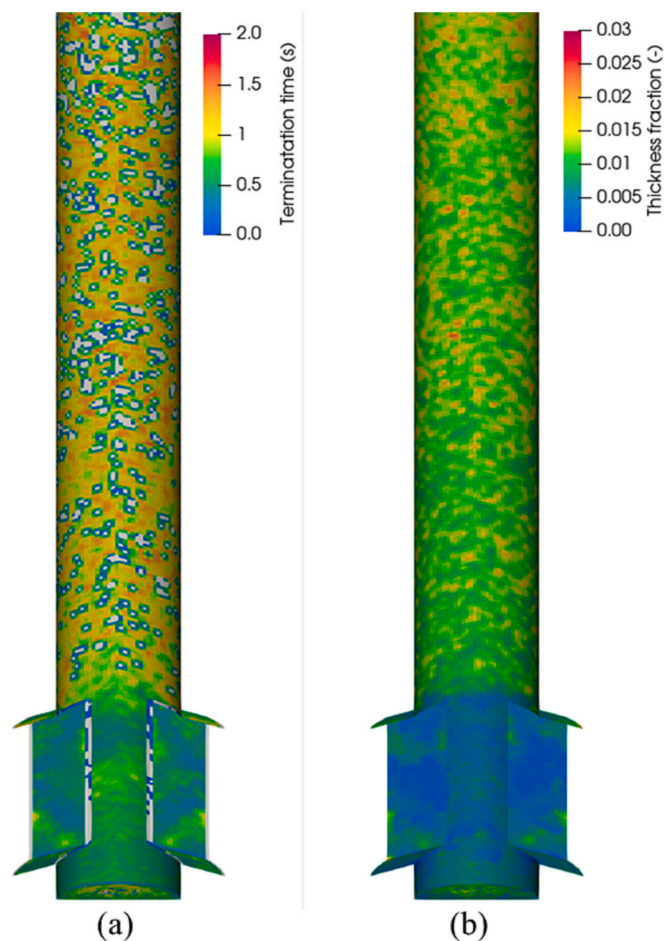


Fig. 6. (a) Termination time of early stage clogging and (b) thickness fraction of the early-stage clogging after 2 s in boundary cells.

the time derivatives of those in Fig. 10(a). To have a better visualization, the fluctuating curves in thin lines have been smoothed and plotted as thick lines. The total deposition and fragmentation rates increased quite fast until 9 min. After that, their increase rates slowed down. After 9 min, since the increase in the total fragmentation rate was larger than that of the total deposition rate, the total clogging rate decreased gradually.

Variation in clog thickness at a certain point in the middle section of the SEN is plotted in Fig. 11. The clog thickness was calculated as the distance from the SEN wall to the clog front. The local clog growth rate was obtained from the time derivative of the local clog thickness. The general trend of the local clog thickness is increasing, but sometimes it decreases shortly. The local clog growth rate frequently has negative values, which indicates fragmentation. This curve demonstrates how frequent fragmentation may occur at a certain point.

4. Comparison with industrial observation of the as-clogged SEN

Inside profile of an as-clogged SEN was obtained with a method of 3D laser scanning. The real clog front and simulated one are compared in Fig. 12. A satisfactory agreement was obtained. The simulated profile of the clog front is quite similar to that of the as-clogged SEN: the asymmetric bowl shape of the clog in the bottom region of the SEN; a thinner clog in the port regions than that in the tube part; a thicker clog in the middle of the tube part of the SEN than in both ends, i.e. a convex profile of the clog front in the tube part. Note that the clog front of the as-clogged SEN was observed after approximately 3 h of casting, whereas the simulated clog formed at around 1 h, hence, the simulated clog

appears thinner than the real one. It should also be mentioned that in the as-clogged SEN, the entrapped steel melt was difficult to be completely drained out after CC operation. Some steel drops can still be observed inside the SEN, especially in the ports area. The clog front in the real SEN has many tiny curvatures, whereas the simulated clog front seems smoother. This might be partially due to the current model, which is volume-average based and it cannot solve the detailed roughness of the clog front.

A direct quantitative comparison between the simulation results and plant data may not be necessary at this moment. One reason is due to the aforementioned difficulty in obtaining the real clog front without steel entrapment; other reasons include the uncertainties of the boundary conditions, process parameters of the CC, and some model assumptions. For instance, the injection rate of NMIs at the inlet is based on a rough estimation of the number density of NMIs under thermodynamically ideal conditions, which might not be fully valid. In the calculation of the critical stress at the sintering neck between alumina particles, it is assumed that the flow velocity is perpendicular to the clog finger, as shown in Fig. 3(c). This assumption works reasonably when one face of the partially-clogged cell is connected to a fully-clogged cell and flow is parallel to the clog. When a partially-clogged cell has two or more interfaces with fully-clogged cells, or when the flow is not parallel to the clog front, the above assumption may lead to an error in estimating the clog growth. This point can explain why the simulated clog front profile in the tube part (where the flow is almost straight and parallel to the wall) is very similar to the real one, and why there is an underestimation of clog volume in the port area (where the flow is very dynamic and multi-directional), as can be seen in Fig. 12. Further discussions continue in the next section.

5. Parameter study and discussions

5.1. Importance of clog fragmentation

To understand the role of the fragmentation in the clogging process, a new simulation was conducted by ignoring the fragmentation, which was compared with the previous (reference) simulation case that has considered the clog fragmentation. An excessively high mechanical strength (100 times larger than the real one) was deliberately assigned to the alumina, so that the clog fingers are hardly broken by the flow. The simulation results of two cases are compared in Fig. 13. By neglecting the clog fragmentation, the clogging develops very rapidly and irregularly. In the tube part of SEN, individual bulges grow horizontally and sometimes form branches. These branches may eventually build a network and form some large pores (\sim cm). From metallographic analysis of the as-clogged SEN, large pores do exist in the clog structure, but they are in the order of mm or smaller. The pore size of \sim cm is unrealistic. Additionally, by ignoring fragmentation the bottom bowl is filled up by clog too quickly.

Fragmentation is a phenomenon which always accompanies the clogging process. During the clog growth, continuous deposition of NMIs builds up the clog structure, whereas fragmentation phenomenon removes mass from the clog structure and slows down the clogging process. This phenomenon has been evidenced by the industry online-monitored CC parameter, Fig. 1(b); the frequent low-down of the stopper rod position indicates the occurrence of the fragmentation. From the modeling results of Fig. 10, one can also see that the mass fragmentation rate increases with the mass deposition rate of the NMIs. If no fragmentation had occurred during CC, the clogging process would occur much sooner. This study confirms the importance of the fragmentation event, and it is necessary to include the fragmentation sub-model in the simulation of the clogging process. However, this sub-model still needs further improvements to simulate clogging phenomena more accurately. Some of the most important ones are addressed in Section 5.4.

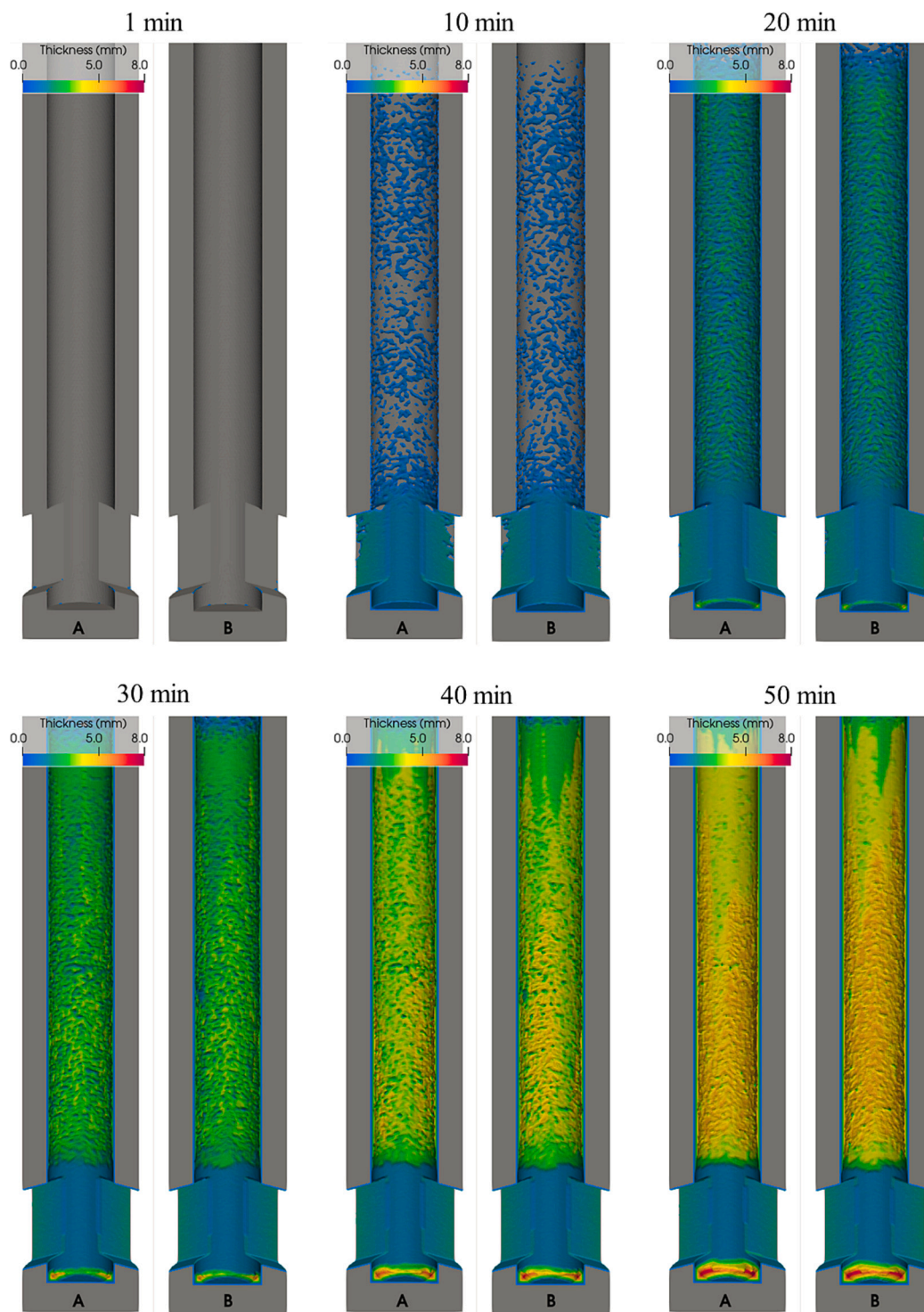


Fig. 7. Evolution of clog in two halves of the SEN.

5.2. Mesh sensitivity

The sensitivity of the modeling result of the clog growth to the mesh size was investigated previously in a laboratory scale [35]. Here, the effect of mesh size on the modeling result of the clogging including fragmentation for a real-size SEN is studied. Computational cells inside the SEN were hexahedron with skewness of 0.127 ± 0.09 . In the base mesh (as reference case), the minimum and maximum cell volume was $3.53 \times 10^{-10} \text{ m}^3$ and $5.04 \times 10^{-9} \text{ m}^3$, respectively. Two other cases were simulated: the cell length size was enlarged 50% (named as 50%

coarser) and reduced 50% (named as 50% finer). The simulation results of 30 min are shown in Fig. 14. In Fig. 14(a), the time evolutions of the total clogging mass seem similarly for all cases, but with different temporal slopes. At 30 min, the total clogging mass is: 0.64 kg in 50% for the coarser mesh, 0.61 kg for the base mesh, and 0.58 kg for the 50% finer mesh. Fig. 14(b) shows the final clog front profiles of the three cases. They are almost similar: a thin layer of clog in the port area, bowl shape of clog at the bottom, and random bulges in the tube part of the SEN. However, case of 50% coarser mesh could not resolve the bowl shape and random bulges well. Base mesh and 50% finer mesh gave very

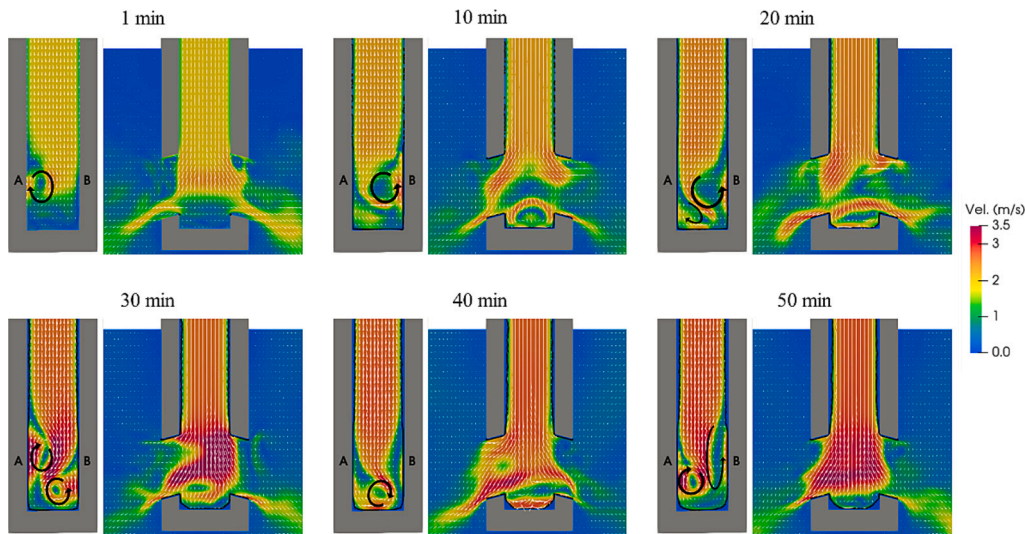


Fig. 8. Melt flow pattern during clogging, showing on two symmetrical planes. Solid line represents the clog front.

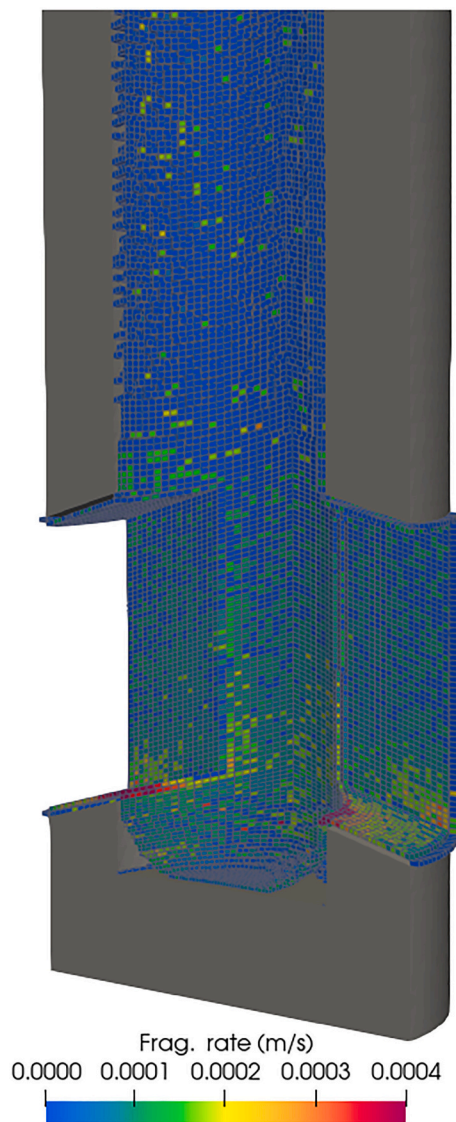


Fig. 9. Local fragmentation rate (g/s) at 50 min, shown on the clog front.

similar results. More details of clog front can be achieved by the 50% finer mesh. The base mesh is fine enough to resolve major profile details of the clog front. Here, effects of mesh size are discussed. Sensitivity of the model to other numerical parameters like, mesh type, and time-step, etc. could be subject of further investigations.

The typical size of NMI particles, which contribute to SEN clogging, is on the order of 10 μm [48] and typical computational cell size is about 1 to 2 orders of magnitude larger. Therefore, the volume average approach has to be considered as the most feasible method for modeling the clogging process. Referring to the postmortem analysis of the as-clogged structure [49], the clog can be treated as a porous medium. However, calculating of the melt flow near the clog front is very difficult due to the random nature of the NMI deposition and the clog structure. In the current model, the permeability in an interface cell, also called a ‘partially-clogged’ cell, was modified by the clog fraction (f_{clog}):

$$K_{\text{per}} = \frac{(1 - \bar{f}_p) (1 - \bar{f}_p^{1/3})}{108 (\bar{f}_p^{1/3} - \bar{f}_p)} D_{\text{pore}}^2 \frac{1}{f_{\text{clog}}^n}, \quad (4)$$

where \bar{f}_p is the average particle (volume) fraction in a fully-clogged region; D_{pore} is the diameter of large pores; and n is an interpolation correction power. K_{per} is used to calculate a Darcy source term in momentum and turbulence equations. The term $\frac{1}{f_{\text{clog}}^n}$ prevents an immediate presence of uniform porous medium with small volume of deposit, i.e. a small increase in f_{clog} . More details of this approach were described previously [35]. $n = 5$ was empirically found to be a proper value. Despite of the above modification to K_{per} , the volume average approach would still lead to some error estimation of the velocity and turbulence in partially-clogged cells. Further improvements are required.

5.3. Effects of turbulence model

Among various turbulence models, scale-adaptive simulation (SAS) was chosen for the reference case because of its stability and its adaptive nature to switches between Reynolds-averaged Navier-Stokes (RANS) and large-eddy simulation (LES) modes depending on the resolved scales in the flow. Shear Stress Transport (SST) $k-\omega$ turbulence model is also a popular model for its robustness and capturing near-wall behavior of flow. Both turbulence models were compared. Total clogging mass during the process for both turbulence models are shown in Fig. 15(a). Two curves are almost similar. Clogging mass of SST $k-\omega$ is slightly larger during most duration of the process. Moreover, SST $k-\omega$ shows larger

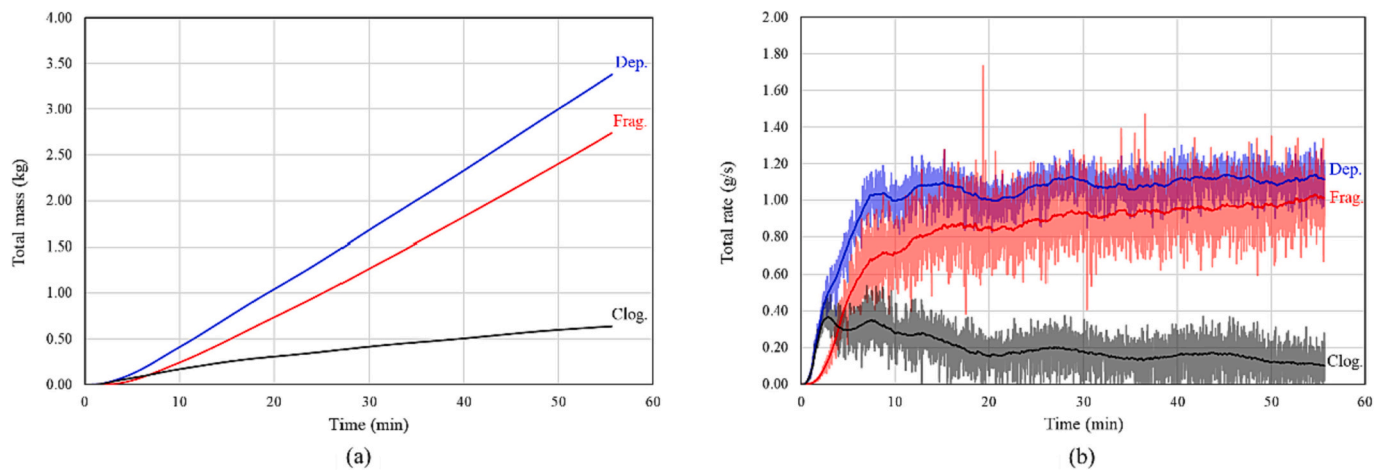


Fig. 10. (a) Mass integrals of deposition, fragmentation, and clogging in the entire SEN as functions of time; (b) the change rates (time derivatives) of them.

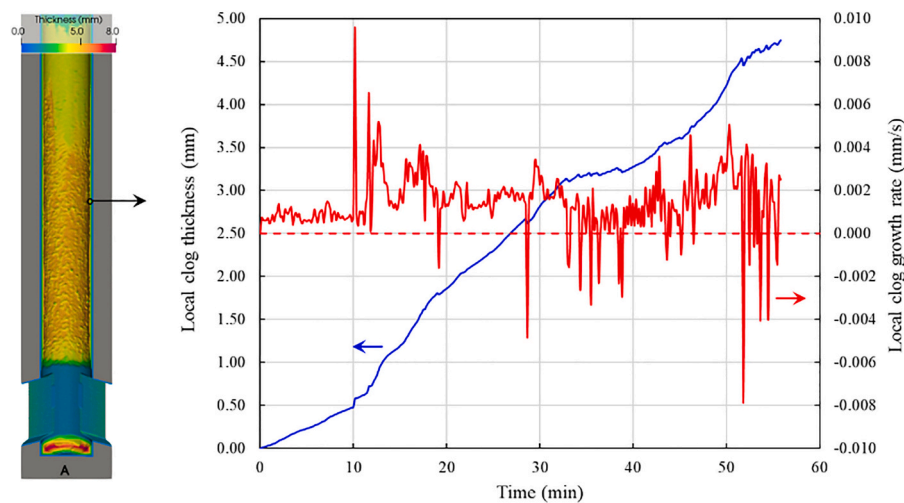


Fig. 11. Local clog thickness and local clog growth rate at a certain point.

changes in the slope than those of SAS. In Fig. 15(b), the clog fronts of two cases after 30 min are quite different. In the tube part of the SEN, SAS predicted tiny random bulges on the clog front, while SST $k-\omega$ made smoother clog front with large bulgy surfaces. At the bottom of the SEN, SST $k-\omega$ model predicted more severe clogging. SST $k-\omega$ might damp excessively turbulent structures, hence less eddies are resolved. As all simulation settings including mesh size in both cases are identical, SAS can predict more detailed clogging than SST $k-\omega$. The calculation cost of two turbulence models was very similar. Therefore, SAS model is recommended for the clogging simulation.

Turbulence results influence the particle tracking and consequently clogging via 'random walk' model, that is a function of turbulence kinetic energy. However, in the near-wall region, a stochastic model [50] is adopted to consider coherent structures which are responsible for particle transport. This model is suitable when the wall surface is fresh and free from any clogging. Hence, it is used for particle tracking in the wall boundary cells and in the bulk of fluid, particle transport is treated by the random walk model [35]. With developing of clogging and changing flow-wall interface, the stochastic model is not valid any more. Therefore, Darcy source term is introduced to the turbulence equations, as explained in the previous section. Finding an accurate source term which can treat momentum and turbulence in a partially-clogged cell using volume average approach should be considered in future developments.

5.4. Other factors influencing clogging and fragmentation

Mechanical strength of alumina under operational conditions is a critical value in the fragmentation sub-model. Some previous works took a value of room temperature (300 MPa) to evaluate the detachment of a sintered alumina particle [14,51], but it is known as temperature dependent [38]. In this paper, 100 MPa was chosen according to the experimental data of mechanical properties of dense alumina and the operating temperature [52].

The interfacial tension (γ) in Eq. (3) is supposed to be the interfacial energy between pure alumina and steel melt. However, it is believed that two approaching alumina particles in the steel melt can rupture the disjoining liquid film between them. Due to the poor wettability of alumina by steel melt, the melt is expelled out of the contact point and a cavity forms around the contact point (sintering point) [51,53,54]. The formation of the cavity results in a capillary force that presses two particles together. The presence of this capillary force influences sintering neck growth between the two alumina particles and leads to faster sintering [47]. This kind of phenomenon is not considered in the current fragmentation sub-model; hence, the sintering neck in this work might be underestimated. In other words, the calculated stress at sintering point is overestimated. Although the general equation of kinetic growth of neck was modified to take non-wettability effects into account [47], it works only for certain cases of large alumina balls (160 μm) composed of

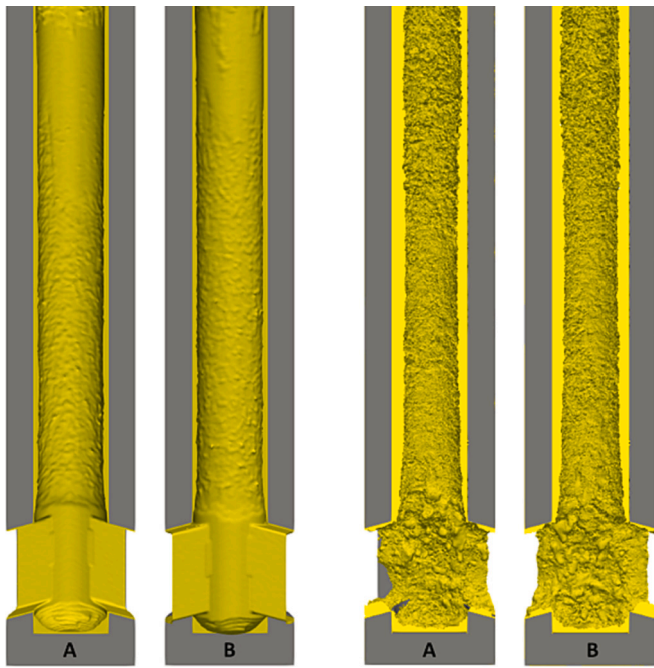


Fig. 12. Comparison of the simulated clog front (left two figures) with clog front of an as-clogged SEN from industry operation (right two figures).

many tiny particles of alumina. Hence, Eq. (3) is subject to further improvement for the case of SEN clogging with small alumina particles in the size of μm .

The current fragmentation sub-model has simplified the network structure of clog as a bunch of clog fingers. The weakest points in this new structure are the bases of virtual sections in each cell. Therefore, the weakest points for all clog fingers in a cell are of the same length. In reality, the clog structure is composed of alumina spheres with different sizes, and weak points of the network are randomly distributed. In other fields of research, more sophisticated models based on force-balance approaches [39] have been proposed, known as multilayer resuspension. Such approaches may be included in future improvements of

fragmentation sub-model to cover natural complexity of clog structure.

Injection of argon gas in the SEN during CC is a popular measure to control the clogging process. The argon gas bubbles can change the flow regime, hence influence NMI deposition and fragmentation; they can also adapt pressure inside the SEN, hence influence the reactions at the steel-refractory interface; they may collect NMIs, even capture the clog fragments and bring them to the slag, etc. For such importance, argon injection in SEN and its effect on clogging are subjects of ongoing research pursued by the present authors for the advancement of the clogging model.

6. Summary

A sub-model was developed to consider the fragmentation phenomenon during SEN clogging in CC of steel. It was integrated in a comprehensive clogging model to simulate the clogging and fragmentation phenomena in a real-scale SEN. The simulated clog profile in the SEN was qualitatively compared with that of the as-clogged SEN, and satisfactory agreement was obtained.

Most important contribution of this work is that the importance of the fragmentation event during SEN clogging was confirmed. Fragmentation always accompanies the clogging process. During the clog growth, continuous deposition of NMIs builds up the clog structure, whereas fragmentation phenomenon removes mass from the clog structure and slows down the clogging process. This phenomenon was evidenced by the industry CC operation via monitored stopper rod position. One can conclude that if no fragmentation had occurred during CC, the clogging process would occur much sooner. It is necessary to include the fragmentation phenomenon in the clogging model.

Finally, the recent status of model development on SEN clogging was discussed. Although an integrated clogging model was presented by the current authors, which has considered most critical steps of clogging, it is still subject to further improvements. Among many other factors influencing the SEN clogging, injection of argon gas was considered as a necessary measure to control the SEN clogging during CC operation. Consideration of argon gas injection is an on-going work of the authors for the advancement of the clogging model.

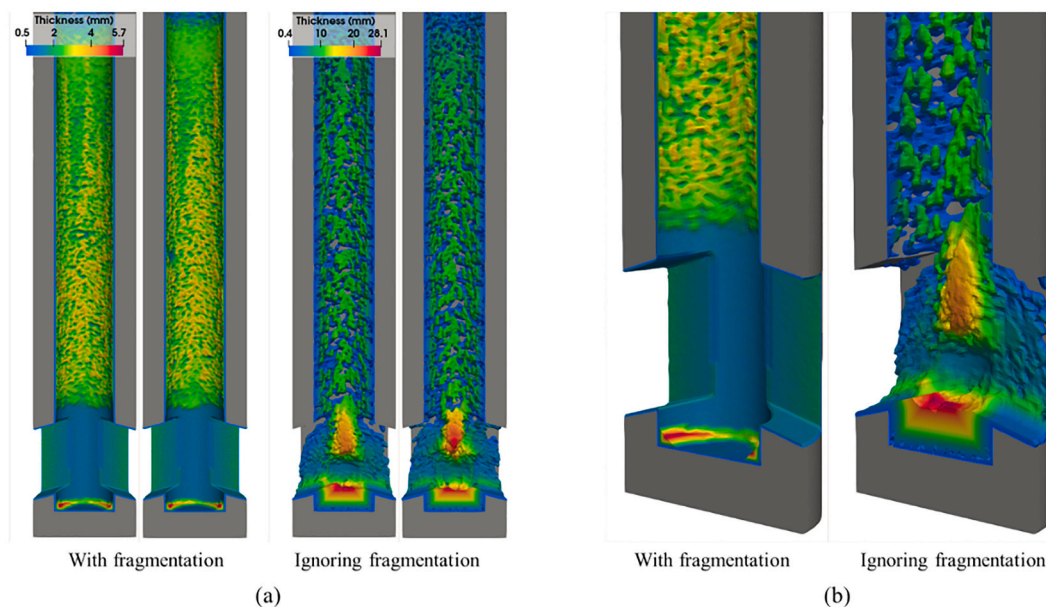


Fig. 13. Comparison of the clog front results in two simulations with and without including fragmentation sub-model: (a) in the whole SEN geometry, (b) zoomed view of port region.

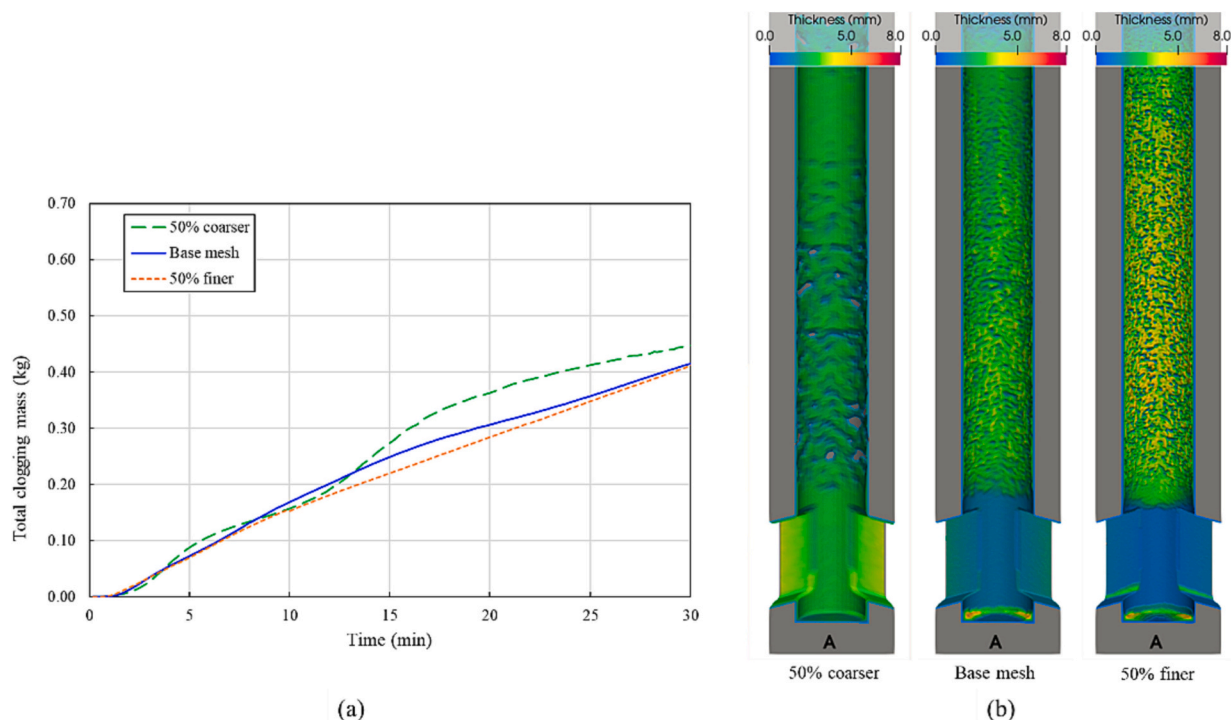


Fig. 14. Mesh sensitivity of the clogging model. (a) Effect of grid size on total clogging mass during the time and (b) final clog front morphology after 30 min.

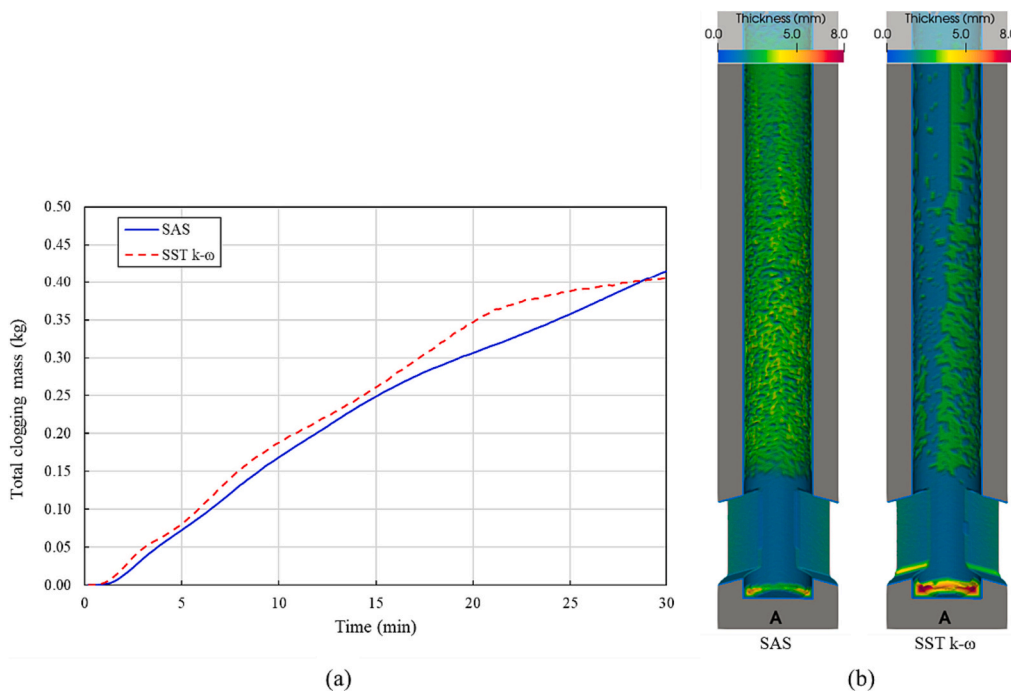


Fig. 15. Effect of turbulence models on (a) the evolution of total clogging mass and (b) the final clog front morphology after 30 min.

Declaration of generative AI and AI-assisted technologies in the writing process

During the preparation of this work the author(s) used ChatGPT-3.5 in order to improve language and readability of some sentences. After using this tool, the author(s) reviewed and edited the sentences as needed and take(s) full responsibility for the content of the publication.

CRediT authorship contribution statement

H. Barati: Conceptualization, Investigation, Methodology, Software, Validation, Visualization, Writing – original draft, Writing – review & editing. **M. Wu:** Methodology, Supervision, Writing – review & editing. **S. Ilie:** Investigation, Resources. **A. Kharicha:** Formal analysis, Software. **A. Ludwig:** Resources, Supervision.

Declaration of Competing Interest

The authors declare that they have no known competing financial interests or personal relationships that could have appeared to influence the work reported in this paper.

Data availability

A part of data is confidential but the rest can be made available on request.

Acknowledgements

The authors gratefully acknowledge the funding support of K1-MET GmbH, metallurgical competence center. The research program of the K1-MET competence center is supported by COMET (Competence Center for Excellent Technologies), the Austrian program for competence centers. COMET is funded by the Federal Ministry for Climate Action, Environment, Energy, Mobility, Innovation, and Technology; the Federal Ministry for Digital and Economic Affairs; the Federal States of Upper Austria, Tyrol, and Styria; and the Styrian Business Promotion Agency (SFG). In addition to the public funding from COMET, this research project was partially financed by scientific partners (Montanuniversität Leoben and Johannes Kepler University Linz) and industrial partners (voestalpine Stahl Linz GmbH, voestalpine Stahl Donawitz GmbH, and RHI Magnesita GmbH). The authors also thank voestalpine Stahl Linz GmbH for providing topography of the as-clogged SEN.

References

- Liu Shihong, Wang Xinhua, Zuo Xiangjun, Wang Yufeng, Zhang Lifeng, Niu Shizhen, Liang Mei, Li Chunzeng, Inclusions, lining materials and nozzle clogging during middle carbon steel billet continuous casting process, *Rev. Met. Paris* 105 (2008) 72–79, <https://doi.org/10.1051/metal:2008017>.
- S.K. Michelic, C. Bernhard, Significance of nonmetallic inclusions for the clogging phenomenon in continuous casting of steel—a review, *Steel Res. Int.* 93 (2022) 2200086, <https://doi.org/10.1002/srin.202200086>.
- C. Henry, J.-P.P. Minier, G. Lefèvre, Towards a description of particulate fouling: from single particle deposition to clogging, *Adv. Colloid Interf. Sci.* 185–186 (2012) 34–76, <https://doi.org/10.1016/j.cis.2012.10.001>.
- J.J. Klemes, O. Arsenyeva, P. Kapustenko, L. Tovazhnyanskyy, *Compact Heat Exchangers for Energy Transfer Intensification*, 1st ed, CRC Press, 2015, <https://doi.org/10.1201/b18862>.
- H. Wang, L. Sheng, J. Xu, Clogging mechanisms of constructed wetlands: a critical review, *J. Clean. Prod.* 295 (2021), 126455, <https://doi.org/10.1016/j.jclepro.2021.126455>.
- E. Commission, D.-G. for Research, Innovation, C. Tscheuschner, S. Ekerot, M. Wu, H. Barati, C. Bernhard, S. Michelic, P. Dorrer, M. Schäperkötter, P. Müller, R. Rössler, G. Xia, *Investigation of the Effect of Ti on Clogging of Feeding Systems and its Prevention for Continuous Slab Casting (TICLOGG)*, final report, Publications Office, 2020.
- J.-H. Lee, M.-H. Kang, S.-K. Kim, Y.-B. Kang, Oxidation of Ti added ULC steel by CO gas simulating interfacial reaction between the steel and SEN during continuous casting, *ISIJ Int.* 58 (2018) 1257–1266, <https://doi.org/10.2355/isijinternational.ISIJINT-2018-164>.
- K. Sasai, Y. Mizukami, Reaction mechanism between alumina graphite immersion nozzle and low carbon steel, *ISIJ Int.* 34 (1994) 802–809, <https://doi.org/10.2355/isijinternational.34.802>.
- Y. Vermeulen, B. Coletti, B. Blanpain, P. Wollants, J. Vleugels, Material evaluation to prevent nozzle clogging during continuous casting of Al killed steels, *ISIJ Int.* 42 (2002) 1234–1240, <https://doi.org/10.2355/isijinternational.42.1234>.
- S. Basu, S.K. Choudhary, N.U. Girase, Nozzle clogging behaviour of Ti-bearing Al-killed ultra low carbon steel, *ISIJ Int.* 44 (2004) 1653–1660, <https://doi.org/10.2355/isijinternational.44.1653>.
- Y. Miki, H. Kitaoka, T. Sakuraya, T. Fujii, Mechanism for separating inclusions from molten steel stirred with a rotating magnetic field, *ISIJ Int.* 32 (1992) 142–149, <https://doi.org/10.2355/isijinternational.32.142>.
- L. Zhang, B.G. Thomas, State of the art in the control of inclusions during steel ingot casting, *Metall. Mater. Trans. B* 37 (2006) 733–761, <https://doi.org/10.1007/s11663-006-0057-0>.
- G.C. Duderstadt, R.K. Iyengar, J.M. Matesa, Tundish nozzle blockage in continuous casting, *JOM* 20 (1968) 89–94, <https://doi.org/10.1007/BF03378699>.
- K.G. Rackers, B.G. Thomas, *Clogging in continuous casting nozzles*, in: 78th Steelmaking Conference Proceedings, 1995, pp. 723–734.
- S. Rödl, H. Schuster, S. Ekerot, G. Xia, N. Veneri, F. Ferro, S. Baragiola, P. Rossi, S. Fera, V. Colla, others, New strategies for clogging prevention for improved productivity and steel quality, 2012, <https://doi.org/10.2777/76864>.
- H. Bai, B.G. Thomas, Turbulent flow of liquid steel and argon bubbles in slide-gate tundish nozzles: part I. Model development and validation, *Metall. Mater. Trans. B* 32 (2001) 253–267, <https://doi.org/10.1007/s11663-001-0049-z>.
- B. Karnasiewicz, E. Zinggere, Observational study of clogging specimens from the Tundish well showing origin and growth of a clog in an Al-killed Ti-alloyed steel cast, *Metall. Mater. Trans. B* 50 (2019) 1704–1717, <https://doi.org/10.1007/s11663-019-01619-8>.
- L.F. Zhang, B.G. Thomas, State of the art in evaluation and control of steel cleanliness, *ISIJ Int.* 43 (2003) 271–291, <https://doi.org/10.2355/isijinternational.43.271>.
- X. Deng, C. Ji, Y. Cui, Z. Tian, X. Yin, X. Shao, Y. Yang, A. McLean, Formation and evolution of macro inclusions in IF steels during continuous casting, *Ironmak. Steelmak.* 44 (2017) 739–749, <https://doi.org/10.1080/03019233.2017.1368958>.
- P. Dorrer, S.K. Michelic, C. Bernhard, A. Penz, R. Rössler, Study on the influence of FeTi-addition on the inclusion population in Ti-stabilized ULC steels and its consequences for SEN-clogging, *Steel Res. Int.* 90 (2019) 1800635, <https://doi.org/10.1002/srin.201800635>.
- H. Bai, B.G. Thomas, Turbulent flow of liquid steel and argon bubbles in slide-gate tundish nozzles: part II. Effect of operation conditions and nozzle design, *Metall. Mater. Trans. B* 32 (2001) 269–284, <https://doi.org/10.1007/s11663-001-0050-6>.
- L. Zhang, Y. Wang, X. Zuo, Flow transport and inclusion motion in steel continuous-casting mold under submerged entry nozzle clogging condition, *Metall. Mater. Trans. B* 39 (2008) 534–550, <https://doi.org/10.1007/s11663-008-9154-6>.
- C. Hua, Y. Bao, M. Wang, Numerical simulation and industrial application of nozzle clogging in bilateral-port nozzle, *Powder Technol.* 393 (2021) 405–420, <https://doi.org/10.1016/j.powtec.2021.07.070>.
- B.G. Thomas, Q. Yuan, S. Mahmood, R. Liu, R. Chaudhary, Transport and entrapment of particles in steel continuous casting, *Metall. Mater. Trans. B* 45 (2014) 22–35, <https://doi.org/10.1007/s11663-013-9916-7>.
- Q. Yuan, B.G. Thomas, S.P. Vanka, Study of transient flow and particle transport in continuous steel caster molds: part I. Fluid flow, *Metall. Mater. Trans. B* 35 (2004) 685–702, <https://doi.org/10.1007/s11663-004-0009-5>.
- Q. Yuan, B.G. Thomas, S.P. Vanka, Study of transient flow and particle transport in continuous steel caster molds: part II. Particle transport, *Metall. Mater. Trans. B* 35 (2004) 703–714, <https://doi.org/10.1007/s11663-004-0010-z>.
- P. Ni, L.T.I. Jonsson, M. Ersson, P.G. Jönsson, On the deposition of particles in liquid metals onto vertical ceramic walls, *Int. J. Multiphase Flow* 62 (2014) 152–160, <https://doi.org/10.1016/j.ijmultiphaseflow.2014.02.002>.
- P. Ni, L.T.I. Jonsson, M. Ersson, P.G. Jönsson, The use of an enhanced Eulerian deposition model to investigate nozzle clogging during continuous casting of steel, *Metall. Mater. Trans. B* 45 (2014) 2414–2424, <https://doi.org/10.1007/s11663-014-0145-5>.
- T. Botelho, G. Medeiros, G.L. Ramos, A. Costa Silva, The application of computational thermodynamics in the understanding and control of clogging and scum in continuous casting of steel, *J. Phase Equilib. Diffus.* 38 (2017) 201–207, <https://doi.org/10.1007/s11669-017-0525-z>.
- J.-H. Lee, M.-H. Kang, S.-K. Kim, J. Kim, M.-S. Kim, Y.-B. Kang, Influence of Al/Ti ratio in Ti-ULC steel and refractory components of submerged entry nozzle on formation of clogging deposits, *ISIJ Int.* 59 (2019) 749–758, <https://doi.org/10.2355/isijinternational.ISIJINT-2018-672>.
- J.-H. Lee, Y.-B. Kang, Growth of initial clog deposits during continuous casting of Ti-ULC steel – formation and reduction of the initial deposits at nozzle/steel interface, *ISIJ Int.* 60 (2020) 426–435, <https://doi.org/10.2355/isijinternational.ISIJINT-2019-384>.
- G. Li, C. Lu, M. Gan, Q. Wang, S. He, Influence of submerged entry nozzle clogging on the flow field and slag entrainment in the continuous casting mold by the physical model, *Metall. Mater. Trans. B Process Metall. Mater. Process. Sci.* 53 (2022) 1436–1445, <https://doi.org/10.1007/s11663-022-02451-3>.
- M.G. González-Solórzano, R.D. Morales, E. Gutiérrez, J. Guarneros, K. Chattopadhyay, Analysis of fluid flow of liquid steel through clogged nozzles: thermodynamic analysis and flow simulations, *Steel Res. Int.* 91 (2020) 2000049, <https://doi.org/10.1002/srin.202000049>.
- H. Barati, M. Wu, S. Michelic, S. Ilie, A. Kharicha, A. Ludwig, Y.-B. Kang, Mathematical modeling of the early stage of clogging of the SEN during continuous casting of Ti-ULC steel, *Metall. Mater. Trans. B* 52 (2021) 4167–4178, <https://doi.org/10.1007/s11663-021-02336-x>.
- H. Barati, M. Wu, A. Kharicha, A. Ludwig, A transient model for nozzle clogging, *Powder Technol.* 329 (2018) 181–198, <https://doi.org/10.1016/j.powtec.2018.01.053>.
- H. Barati, M. Wu, T. Holzmann, A. Kharicha, A. Ludwig, Simulation of non-metallic inclusion deposition and clogging of nozzle, in: L. Nastac, K. Pericleous, A.S. Sabau, L. Zhang, B.G. Thomas (Eds.), *CFD Modeling and Simulation in Materials Processing 2018*, Springer International Publishing, Cham, 2018, pp. 149–158.
- H. Barati, M. Wu, A. Kharicha, A. Ludwig, Calculation accuracy and efficiency of a transient model for submerged entry nozzle clogging, *Metall. Mater. Trans. B* 50 (2019) 1428–1443, <https://doi.org/10.1007/s11663-019-01551-x>.
- R. Sambasivam, Clogging resistant submerged entry nozzle design through mathematical modelling, *Ironmak. Steelmak.* 33 (2006) 439–453, <https://doi.org/10.1179/174328106X118198>.
- C. Henry, J.P. Minier, Progress in particle resuspension from rough surfaces by turbulent flows, *Prog. Energy Combust. Sci.* 45 (2014) 1–53, <https://doi.org/10.1016/j.pecs.2014.06.001>.

- [40] R. Measures, S. Tait, Quantifying the role of bed surface topography in controlling sediment stability in water-worked gravel deposits, *Water Resour. Res.* 44 (2008), <https://doi.org/10.1029/2006WR005794>.
- [41] H. Friess, G. Yadigaroglu, Modelling of the resuspension of particle clusters from multilayer aerosol deposits with variable porosity, *J. Aerosol Sci.* 33 (2002) 883–906, [https://doi.org/10.1016/S0021-8502\(02\)00049-6](https://doi.org/10.1016/S0021-8502(02)00049-6).
- [42] M. Tregnaghi, A. Bottacin-Busolin, S. Tait, A. Marion, Stochastic determination of entrainment risk in uniformly sized sediment beds at low transport stages: 2. Experiments, *J. Geophys. Res. Earth Surf.* 117 (2012), <https://doi.org/10.1029/2011JF002135>.
- [43] M. Tregnaghi, A. Bottacin-Busolin, A. Marion, S. Tait, Stochastic determination of entrainment risk in uniformly sized sediment beds at low transport stages: 1. Theory, *J. Geophys. Res. Earth Surf.* 117 (2012), <https://doi.org/10.1029/2011JF002134> n/a-n/a.
- [44] K. Iimura, S. Watanabe, M. Suzuki, M. Hirota, K. Higashitani, Simulation of entrainment of agglomerates from plate surfaces by shear flows, *Chem. Eng. Sci.* 64 (2009) 1455–1461, <https://doi.org/10.1016/j.ces.2008.10.070>.
- [45] D. Janis, A. Karasev, R. Inoue, P.G. Jönsson, A study of cluster characteristics in liquid stainless steel and in a clogged nozzle, *Steel Res. Int.* 86 (2015) 1271–1278, <https://doi.org/10.1002/srin.201400316>.
- [46] J. Pilling, A. Hellawell, Mechanical deformation of dendrites by fluid flow, *Metall. Mater. Trans. A* 27 (1996) 229–232, <https://doi.org/10.1007/BF02647763>.
- [47] M. Nakamoto, T. Tanaka, M. Suzuki, K. Taguchi, Y. Tsukaguchi, T. Yamamoto, Effects of interfacial properties between molten Iron and alumina on neck growth of alumina balls at sintering in molten Iron, *ISIJ Int.* 54 (2014) 1195–1203, <https://doi.org/10.2355/isijinternational.54.1195>.
- [48] L. Zhang, W. Pluschkell, Nucleation and growth kinetics of inclusions during liquid steel deoxidation, *Ironmak. Steelmak.* 30 (2003) 106–110, <https://doi.org/10.1179/030192303225001766>.
- [49] H. Barati, M. Wu, A. Kharicha, A. Ludwig, Role of solidification in submerged entry nozzle clogging during continuous casting of steel, *Steel Res. Int.* 91 (2020) 2000230, <https://doi.org/10.1002/srin.202000230>.
- [50] M. Guingo, J.-P. Minier, A stochastic model of coherent structures for particle deposition in turbulent flows, *Phys. Fluids* 20 (2008), 053303, <https://doi.org/10.1063/1.2908934>.
- [51] K. Uemura, M. Takahashi, S. Koyama, M. Nitta, Filtration mechanism of non-metallic inclusions in steel by ceramic loop filter, *ISIJ Int.* 32 (1992) 150–156, <https://doi.org/10.2355/isijinternational.32.150>.
- [52] R.M. Spriggs, J.B. Mitchell, T. Vasolos, Mechanical properties of pure, dense aluminum oxide as a function of temperature and grain size, *J. Am. Ceram. Soc.* 47 (1964) 323–327, <https://doi.org/10.1111/j.1151-2916.1964.tb12994.x>.
- [53] F. Heuzeroth, J. Fritzsche, E. Wertzner, M.A.A. Mendes, S. Ray, D. Trimis, U. A. Peuker, Viscous force - an important parameter for the modeling of deep bed filtration in liquid media, *Powder Technol.* 283 (2015) 190–198, <https://doi.org/10.1016/j.powtec.2015.05.018>.
- [54] K. Sasai, Y. Mizukami, Mechanism of alumina adhesion to continuous caster nozzle with Reoxidation of molten steel, *ISIJ Int.* 41 (2001) 1331–1339, <https://doi.org/10.2355/isijinternational.41.1331>.